The Astrophysical Journal, 700:56–62, 2009 July 20 doi:10.1088/0004-637X/700/1/56


# REAL-TIME OPTICAL SPECTROSCOPY OF VACUUM ULTRAVIOLET IRRADIATED PYRENE:$H_2O$ INTERSTELLAR ICE

J. Bouwman[1], D. M. Paardekooper[1], H. M. Cuppen[1], H. Linnartz[1], and L. J. Allamandola[2]
[1] Raymond & Beverly Sackler Laboratory for Astrophysics, Leiden Observatory, University of Leiden, NL-2300 RA Leiden, The Netherlands; bouwman@strw.leidenuniv.nl
[2] NASA-Ames Research Center, Space Science Division, Mail Stop 245-6, Moffett Field, CA 94035, USA
*Received 2008 September 22; accepted 2009 May 12; published 2009 June 30*

## ABSTRACT

This paper describes a near-UV/VIS study of a pyrene:$H_2O$ interstellar ice analogue at 10 K using optical absorption spectroscopy. A new experimental approach makes it possible to irradiate the sample with vacuum ultraviolet (VUV) light (7–10.5 eV) while simultaneously recording spectra in the 240–1000 nm range with subsecond time resolution. Both spectroscopic and dynamic information on VUV processed ices are obtained in this way. This provides a powerful tool to follow, in situ and in real time, the photophysical and photochemical processes induced by VUV irradiation of a polycyclic aromatic hydrocarbon containing inter- and circumstellar ice analogue. Results on the VUV photolysis of a prototype sample—strongly diluted pyrene in $H_2O$ ice—are presented. In addition to the pyrene cation ($Py^+$), other products—hydroxypyrene (PyOH), possibly hydroxypyrene cation ($PyOH^+$), and pyrene/pyrenolate anion ($Py^-/PyO^-$)—are observed. It is found that the charge remains localized in the ice, also after the VUV irradiation is stopped. The astrochemical implications and observational constraints are discussed.

*Key words:* astrochemistry – ISM: molecules – methods: laboratory – molecular processes

*Online-only material:* color figures

## 1. INTRODUCTION

At present, more than 150 different inter- and circumstellar molecules have been observed in space. The chemical diversity is striking, and both simple and very complex as well as stable and transient species have been detected. Among these unambiguously identified species polycyclic aromatic hydrocarbon (PAH) molecules are lacking even though PAHs are generally thought to be ubiquitous in space (e.g., van Dishoeck 2004). Strong infrared emission features at 3.3, 6.2, 7.7, 8.6, and 11.2 $\mu$m are common in regions of, for example, massive star formation and have been explained by PAH emission upon electronic excitation by vacuum ultraviolet (VUV) radiation. Consequently, PAHs are expected to play a key role in the heating of neutral gas through the photoelectric effect. PAHs are also considered as important charge carriers inside dense molecular clouds, and relevant for molecule formation through ion–molecule interactions (Gillett et al. 1973; Puget & Leger 1989; Allamandola et al. 1989; Kim et al. 2001; Smith et al. 2007; Draine et al. 2007). Nevertheless, the only aromatic species unambiguously identified in space is benzene, following infrared observations (Cernicharo et al. 2001).

In recent years electronic transitions of PAH cations have been studied in the gas phase with the goal to link laboratory data to unidentified optical absorption features observed through diffuse interstellar clouds. Following matrix isolation spectroscopic work (Salama & Allamandola 1991), gas phase optical spectra have been recorded for several PAH cations (Romanini et al. 1999; Bréchignac & Pino 1999) by combining sensitive spectroscopic techniques and special plasma expansions (Motylewski et al. 2000; Linnartz 2009). Such optical spectra have unique features and therefore provide a powerful tool for identifying PAHs in space. So far, however, no overlap has been found between laboratory spectra of gaseous $PAHs^+$ and astronomical features.

In dense molecular clouds, most PAHs should quickly condense onto the $H_2O$-rich icy grain mantles, quenching the IR emission process. Here, they will participate in ice grain chemistry. More than 25 years of dedicated studies, mainly in the infrared, have proven that a direct comparison between laboratory and astronomical ice spectra paints an accurate picture of the composition and the presence of inter- and circumstellar ices, even though solid-state features are rather broad. The spectral features (band position, bandwidth (FWHM), and the intensity ratio of fundamental vibrations) depend strongly on mixing ratio and ice matrix conditions and this provides a sensitive analytical tool to identify ice compositions in space (e.g., Boogert et al. 2008; Öberg et al. 2008).

In the past, several experiments have been reported in which the formation of new molecules was proven upon VUV irradiation of astronomical ice mixtures, typically under high vacuum conditions (e.g., Mendoza-Gomez et al. 1995; Bernstein et al. 1999; Gudipati & Allamandola 2003; Ruiterkamp et al. 2005; Peeters et al. 2005; Elsila et al. 2006). Many of these studies were not in situ, i.e., reactants were determined after warm up of the ice, and although VUV-induced photochemistry at low temperatures is expected to take place, it is not possible to fully exclude that at least some of the observed reactants may have been formed during the warm-up stage. More recently, in situ studies have become possible using ultra high vacuum setups in which ices are grown with monolayer precision and reactions are monitored using reflection absorption infrared spectroscopy and temperature programmed desorption. Recent results show that H-atom bombardment of CO and $O_2$ ice results in the efficient formation of $H_2CO/CH_3OH$ and $H_2O_2/H_2O$, respectively (Watanabe & Kouchi 2002; Ioppolo et al. 2008; Fuchs et al. 2009; Miyauchi et al. 2008). Overall, such studies are still restricted to the formation of rather small species, with ethanol as the most complex molecule investigated in this way (Bisschop et al. 2007). Moreover, the reactants and products should not have overlapping bands in order to track them separately.

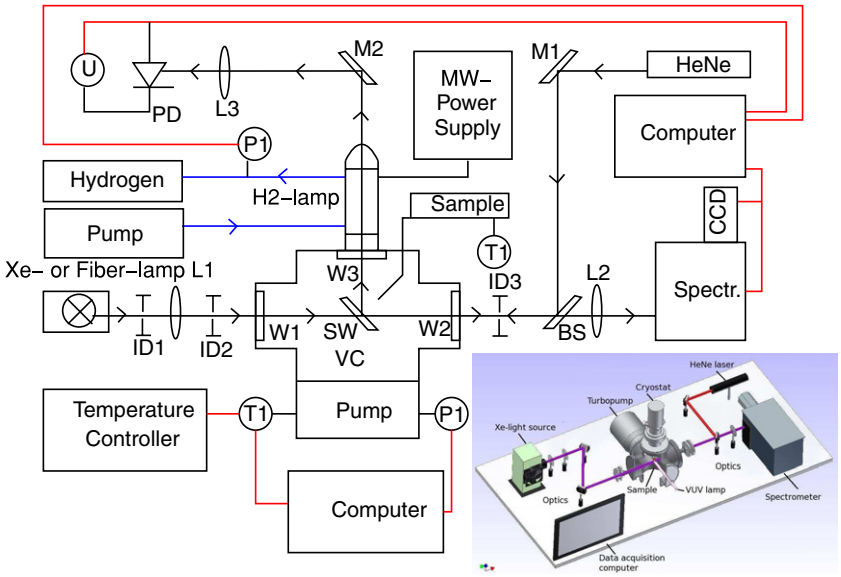


**Figure 1.** Schematic drawing of the experimental setup. BS: beam splitter; IDX: iris diaphragm X; LX: lens X; MX: mirror X; PD: photo diode to monitor interference fringes; PI: pressure indicator; SW: $MgF_2$ cold sample window; TI: temperature indicator; U: voltage meter; VC: vacuum chamber; and WX: $MgF_2$ window X. The light paths are indicated by arrows, the data wiring is indicated in red lines, and the hydrogen flow is indicated by blue lines (see online color version). The inset shows a three-dimensional drawing of the experimental setup.

(A color version of this figure is available in the online journal.)

In the present work, a new approach is presented that extends our previous FTIR work on interstellar ice analogues to the UV/VIS. With the new setup it is possible to record, in situ, the VUV photochemistry of PAHs and PAH derivatives in water ice at 10 K in real time. In the next section, this new approach is discussed in detail. The first results for the PAH pyrene ($C_{16}H_{10}$, or Py) and its photoproducts, pyrene cation ($C_{16}H_{10}^+$, or $Py^+$), hydroxypyrene (PyOH), hydroxypyrene cation ($PyOH^+$), and pyrene/pyrenolate anion ($Py^-/PyO^-$) in $H_2O$ ice are presented in Section 3. Finally, the astrophysical relevance of this work is discussed in Section 5. The latter is twofold. First, time-dependent results of VUV irradiated ice provide general insight into possible reaction pathways upon photoprocessing of PAH containing water ice. Second, the results provide a spectroscopic alternative to search for PAH and PAH-related optical features in the inter- and circumstellar medium (ISM/CSM) through electronic solid-state absorptions.

## 2. EXPERIMENTAL

A schematic of the experimental setup is shown in Figure 1. The experiment consists of three units: a vacuum chamber in which the ice is grown, a special VUV irradiation source that is used for the photoprocessing of the ice and a source-emitting broadband light that is focused into the ice and subsequently detected using a monochromator equipped with a sensitive CCD camera.

The vacuum chamber consists of an ISO-160 6-cross piece. A 300 l $s^{-1}$ turbomolecular pump, backed by a 10 $m^3$ $hr^{-1}$ double stage rotary pump, is used to evacuate the chamber and to guarantee an operating pressure of $\sim 10^{-7}$ mbar. A catalytic trap is mounted on the pre-vacuum pump to prevent pump oil from entering the vacuum chamber.

The top flange of the cross piece holds a differentially pumped rotary flange on which is mounted a closed cycle helium refrigerator equipped with a cold finger. A $MgF_2$ sample window with a diameter of 14 mm, clamped into an oxygen-free copper holder between indium gaskets, is mounted on the cold finger and centered on the optical axis of the setup. This allows for rotation of the sample window through 360° under vacuum. The sample window can be cooled down to 10 K and a thermocouple (Chromel-Au/Fe (0.07%)) and a temperature controller guarantee accurate temperature settings with 0.1 K precision.

The Py:$H_2O$ sample is prepared by vapor depositing pyrene from a solid sample (Aldrich 99%) heated to 40°C, together with milli-Q water vapor from a liquid sample. The entire inlet system is maintained at $\geqslant$40°C during deposition and comprises gas bulbs containing the sample material and tubing for directed deposition, approximately 15 mm from the sample window. The flow rate of the sample material is set by a high precision dosing valve. Condensation inside the tube is prohibited by additional resistive heating and the temperature settings are monitored by K-type thermocouples. The resulting ice film thickness is accurately measured by recording the number of interference fringe maxima ($m$) of a HeNe laser ($\lambda = 632.8$ nm) which strikes the sample window at an angle of $\theta = 45°$. To monitor film growth and thickness, the intensity of the reflected laser light is measured with a sensitive photodiode. The ice thickness is subsequently determined by:

$$d = \frac{m\lambda_{\mathrm{HeNe}}}{2n_{\mathrm{ice}}\cos\theta}, \quad (1)$$

with the refractive index of the predominantly $H_2O$ ice being $n_{\mathrm{ice}} \approx 1.3$. This is illustrated in Figure 2 where both interference fringes produced during ice deposition and the simultaneous growth of the integrated neutral Py absorbance band are shown. The final ice thickness amounts to 1.7 $\mu$m and is reproducible to within 5% or better. Simultaneously, the number of pyrene molecules in the ice sample ($N$) is monitored by measuring the integrated absorbance of its strongest transition ($S_2 \leftarrow S_0$) (see Figure 2). The number of pyrene molecules per $cm^2$ can be calculated via (Kjaergaard et al. 2000; Hudgins et al. 1993):

$$N = \frac{\int_{\nu_1}^{\nu_2} \tau \, d\nu}{8.88 \times 10^{-13} f}, \quad (2)$$

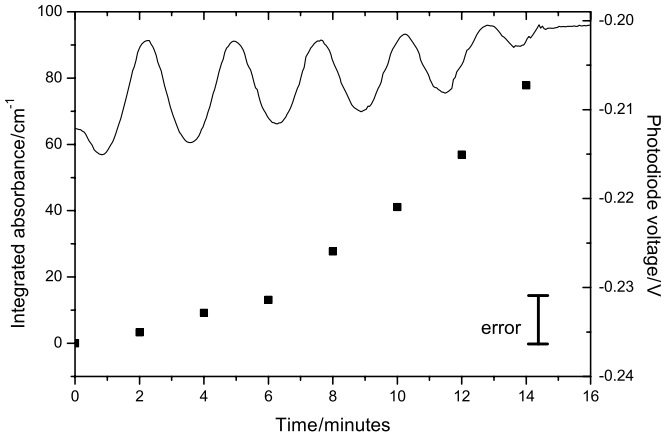


**Figure 2.** Growth of the integrated pyrene absorption band (squares and left axis) and the interference fringes measured by the photodiode (right axis). At $t = 14$ minutes, the deposition is stopped and the interference pattern diminishes. The error bar shown in the right lower corner applies to the pyrene-integrated absorbance.

where $f = 0.33$ is the known oscillator strength of the $S_2 \leftarrow S_0$ transition of pyrene (Bito et al. 2000; Wang et al. 2003). The resulting column density of pyrene molecules amounts to about $4 \times 10^{14}$ cm$^{-2}$. For a typical sample with a thickness of 1.7 $\mu$m, the column density of $H_2O$ molecules amounts to $4 \times 10^{18}$ cm$^{-2}$, using the value for the density of amorphous ice ($\rho = 0.94$ g cm$^{-3}$; Sceats & Rice 1982). Thus, the sample is calculated to consist of a 1:10,000 pyrene:$H_2O$ mixture. This mixing ratio can be roughly varied by changing the $H_2O$ flow rate or the pyrene sample temperature. The HeNe beam used here for monitoring the ice growth process also traces other elements along the optical path and is used to align all components.

The vacuum UV radiation from a special microwave (MW) powered hydrogen discharge lamp is used to simulate the interstellar radiation field (Muñoz Caro et al. 2002). The lamp consists of a flow tube clamped in a McCarroll cavity (McCarroll 1970) and emits mainly Ly-$\alpha$ radiation around 121.6 nm and, with less intensity, a band centered around 160 nm. The cavity is excited by a regular MW power supply (100 W, 2450 MHz). The $H_2$ pressure in the lamp is maintained at 0.4 mbar during operation (Praxair 5.0 $H_2$). This results in a VUV photon flux of $\sim 10^{15}$ photons cm$^{-2}$ s$^{-1}$. The lamp is centered onto the front flange and the VUV radiation enters the setup toward the ice sample through a $MgF_2$ window that also serves as a vacuum seal. A shutter is used to block the VUV until the moment that the ice processing should start. Besides eliminating the need to switch the $H_2$ lamp on and off during the course of an experiment, this allows the lamp to stabilize before irradiation starts. This is important when tracking photochemical behavior during extended periods of photolysis.

A 300 W ozone-free Xe-arc lamp serves as a broadband white light source to measure the spectral ice features in direct absorption. The lamp has a spectral energy distribution that covers the full detector range (200 nm $< \lambda <$ 2400 nm). Alternatively, the light from a halogen fiber lamp can be used when no UV coverage is desired. An optical system consisting of lenses and diaphragms is used to guide the light beam through a $MgF_2$ window along the optical axis—coinciding with the pre-aligned HeNe beam—and crossing the ice sample at a 45° angle. Light that is not absorbed exits the vacuum chamber through a second $MgF_2$ window after which it is focused onto the entrance slit of an ANDOR Shamrock spectrometer. The spectrometer is equipped with two interchangeable turrets which holds four gratings in total (2400, 1200, 600, and 150 lines mm$^{-1}$), allowing for a trade-off between wavelength coverage and spectral resolution, depending on the experimental needs. Since typical ice absorption bands exhibit a FWHM of 4–20 nm, most of the experiments are performed using the 600 lines mm$^{-1}$ grating, resulting in an accessible wavelength range of ~140 nm.

The light is dispersed onto a very sensitive 1024 × 256 pixel CCD camera with 16-bit digitization. The resulting signal is read out in the vertical binning mode by a data acquisition computer. Spectra are taken in absorbance mode ($\tau = -\ln(I/I_0)$) with respect to a reference spectrum ($I_0$) taken directly after depositing the sample. Recording a single spectrum typically takes about 5 ms and spectra are generally co-added to improve the signal-to-noise ratio (S/N). In a typical experiment more than 1000 individual spectra are recorded and are reduced using LabView routines. Data reduction consists of local linear baseline corrections, multiple Gaussian fitting of absorption profiles and absorption band integration.

## 3. SPECTROSCOPIC ASSIGNMENT

Figure 3 shows the 310–500 nm spectrum of a Py:$H_2O$ ice at 10 K after 1200 s of in situ photolysis in absorbance mode. The spectrum is baseline subtracted and given in optical depth (OD). Since the spectrum recorded before VUV irradiation is taken as a reference ($I_0$), bands with positive OD values arise from species produced by photolysis while the carriers of negative OD bands decrease in density. It is noteworthy that S/Ns are good even though the processes are studied in a very dilute mixture (Py:$H_2O$ ~1:10,000). Previous work was on more concentrated samples (PAH:$H_2O$ ~1:500, Gudipati & Allamandola 2003; PAH:$H_2O$ ~1:800 to 1:3200, Bernstein et al. 1999).

A Gaussian fit to all of the features visible in the spectrum is indicated as well. Clearly, a number of new species are produced at the expense of neutral pyrene. The peak positions, FWHM and assignments of all the bands in Figure 3 are summarized in Table 1, along with comparisons of earlier results found in other molecular environments. The assignments given in Figure 3 were made as follows. Based on previous studies of pyrene in rare gas matrices (Vala et al. 1994; Halasinski et al. 2005), the strong, negative band peaking at 334 nm is readily assigned to the $^1B_{2u} \leftarrow {}^1A_g$ electronic transition of neutral pyrene ($S_2 \leftarrow S_0$). Similarly, the positive bands near 363, 446, and 490 nm are assigned as the strongest members of the pyrene cation $^2B_{1u} \leftarrow {}^2B_{3g}$, $^2A_u \leftarrow {}^2B_{3g}$ and $^2B_{1u} \leftarrow {}^2B_{3g}$ vibronic transitions, respectively (Vala et al. 1994; Hirata et al. 1999). Table 1 shows that the bandwidth (FWHM) of the $Py^+$ bands is broader in the solid $H_2O$ than in rare gas matrices, in accordance with the stronger interactions within the $H_2O$ matrix network. Similarly, larger shifts in peak position may be expected.

In addition to the $Py^+$ bands, other new bands appear near 345, 367, 405, and 453 nm. We ascribe these to hydroxypyrene (PyOH), hydroxypyrene cation ($PyOH^+$), and pyrene/pyrenolate anion ($Py^-/PyO^-$) based on the work of Milosavljevic & Thomas (2002) who reported the spectra of 1-hydroxypyrene and its daughter products in various media. The suggestion of anion production in these ices is noteworthy in view of the astronomical detection of negative ions both in the solid state (van Broekhuizen et al. 2005) and in the gas phase (e.g., Agúndez et al. 2008).

The appearance of clear bands due to PyOH, $PyOH^+$, and $Py^-/PyO^-$ after VUV radiation at 10 K is somewhat surprising. Previous optical studies of the VUV photolysis of three different

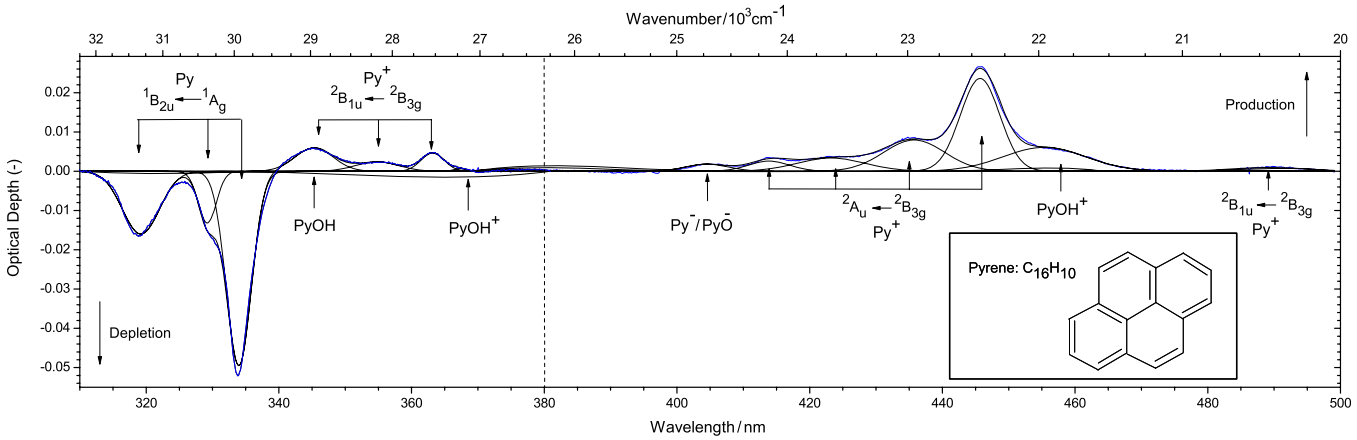


**Figure 3.** Baseline corrected spectrum obtained after 1200 s of VUV irradiation of a pyrene:$H_2O$ ice at 10 K. The absorption features in the plot are assigned and fitted with Gaussian profiles. A negative OD indicates species destruction, a positive OD species formation. The left spectrum (up to 280 nm) is scaled down by 30% to facilitate comparison.

(A color version of this figure is available in the online journal.)

**Table 1**
Vibronic Bands of Pyrene and Its Photoproducts in a $H_2O$ Ice Compared with Rare Gas Matrix Literature Values

| Species | State | $\lambda_{H_2O}$(nm) | FWHM (nm) | $\lambda_{lit.}$ (nm) | $FWHM_{lit.}$ (nm) | $\lambda_{H_2O} - \lambda_{rg}$ | ΔFWHM |
|---|---|---|---|---|---|---|---|
| Py | $^1B_{2u}$ | 334.0 | 4.4 | 323.3[a] | n.a. | 10.7 | ... |
| | | 329.2 | 3.2 | 319.1[a] | n.a. | 10.1 | ... |
| | | 319.2 | 6.5 | 309.4[a] | n.a. | 9.8 | ... |
| $Py^+$ | $^2B_{1u}$ | 363.2 | 3.6 | 362.6[b] | 2.2 | 0.6 | 1.4 |
| | | 354.0 | 6.5 | 355.1[b] | 2.1 | −1.1 | 4.4 |
| | | 344.9 | 6.2 | ... | ... | ... | ... |
| $Py^+$ | $^2A_u$ | 445.6 | 6.6 | 443.8[b] | 4.5 | 1.8 | 2.1 |
| | | 435.5 | 10.2 | 433.2[b] | 4.3 | 2.3 | 5.9 |
| | | 423.0 | 12.2 | 422.9[b] | 4.1 | 0.1 | 8.1 |
| | | 413.8 | 5.3 | 412.1[b] | 3.9 | 1.7 | 1.4 |
| $Py^+$ | $^2B_{1u}$ | 490.1 | 10.0 | 486.9[b] | 5.5 | 3.2 | 4.5 |
| PyOH | | 344.9 | 5.8 | 340[c] | ... | ... | ... |
| $Py^-/PyO^-$ | | 405.2 | 7.3 | 410[c] | ... | ... | ... |
| $PyOH^+$ | | 366.8 | 3.0 | ... | ... | ... | ... |
| $PyOH^+$ | | 452.9 | 18.2 | 465[c] | ... | ... | ... |

**Notes.**
[a] Values measured in a Ne matrix taken from Halasinski et al. (2005).
[b] Values measured in an Ar matrix taken from Vala et al. (1994).
[c] Values measured in $H_2O$ and 2-chlorobutane taken from Milosavljevic & Thomas (2002).

PAHs in $H_2O$ ice indicated that conversion of the parent neutral PAH to the cation was the major, and apparently only, photolytic step and that the cation remained stabilized in the ice to remarkably high temperatures (∼100 K) for long periods (e.g., Gudipati & Allamandola 2006). Gudipati (2004) further showed that, in the case of naphthalene (Nap), subsequent reactions between $Nap^+$ and the $H_2O$ matrix did indeed produce NapOH, but only during warm-up (∼100 K). Using mass spectroscopy, Bernstein et al. (1999) showed that PAH oxides and hydroxides were part of the residues left *after* VUV photolyzed PAH/$H_2O$ ices were warmed under vacuum. Furthermore, upon prolonged exposure, the VUV transmittance of the $MgF_2$ hydrogen lamp window drops and with this the PyOH and $PyOH^+$ production also decreases relative to the production of $Py^+$. This suggests that photolytic processes within the pyrene containing water ice change, perhaps because water dissociation becomes less effective with reduced hard UV flux while direct Py ionization still readily occurs with near UV photons (Gudipati & Allamandola 2004). The influence of temperature and UV spectral energy distribution is currently under investigation.

## 4. CHEMICAL EVOLUTION OF THE ICE

To further investigate the spectroscopy and the photochemistry of VUV irradiated $H_2O$-rich ices that contain PAHs, time-dependent optical studies were performed. Figure 4 shows the integrated OD behavior of the Py, $Py^+$ (for two bands), and PyOH absorptions as function of photolysis time. During the first 130 s of VUV irradiation, the Py decay is clearly correlated with $Py^+$ growth. This allows us to determine relative band strengths of the two species by investigation of the short timescale correlation. The subsecond time response of the present setup is a prerequisite for this to work. We derive a band strength of $2.9 \times 10^{-13}$ cm molecule$^{-1}$ for the $^2A_{2u} \leftarrow {}^2B_{3g}$ $Py^+$ transition in $H_2O$ ice using Equation (2). As other chemical processes become important, the correlation disappears. The loss of Py slows significantly while the $Py^+$ starts a slow decline after the maximum is reached. The PyOH signal continues to grow slowly but steadily throughout the photolysis process and is most likely formed by $Py/Py^+$ reacting with photoproducts of $H_2O$. Its formation is consistent with the recent outcome of a quantitative VUV photodesorption study of $H_2O$ ice under

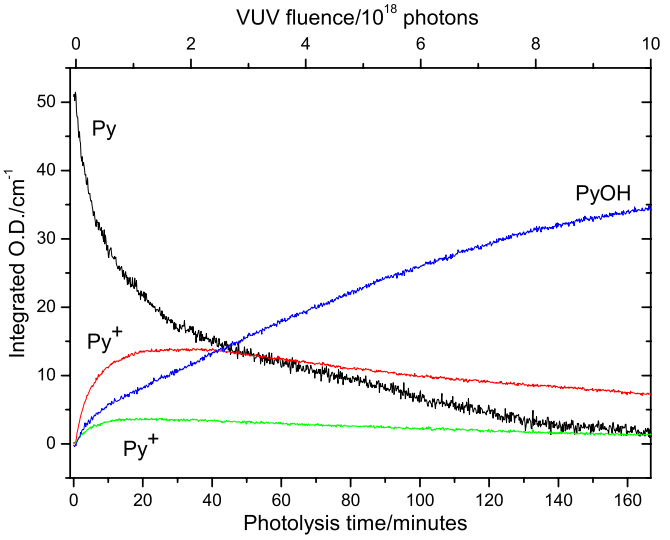


**Figure 4.** Behavior of Py, $Py^+$ (two transitions), and PyOH as a function of VUV photolysis time/VUV fluence.

(A color version of this figure is available in the online journal.)

ultra high vacuum conditions, where a H+OH photodissociation channel was reported (Öberg et al. 2009). A reaction network connecting all of these species is presented in Figure 5.

In addition to $Py^+$ formation and reactivity during irradiation, we have also studied its stability within the ice when photolysis is stopped. Figure 6 plots the normalized integrated OD of the 445.6 nm $Py^+$ band as a function of time after VUV radiation is stopped. The figure spans 50 hr and shows that although the total $Py^+$ signal drops, 60% remains trapped in the ice after 2 days. The small wiggle at the 0.05 level is due to baseline variations. There are clearly two decay channels, one "fast" and one "slow". The following expression is used to fit the experimental data:

$$y = A_1 \exp(-t/\tau_1) + A_2 \exp(-t/\tau_2), \quad (3)$$

with $A_1 = 0.70$, $\tau_1 = 351.3$ hr, $A_2 = 0.22$, and $\tau_2 = 1.7$ hr. This produces the red curve in Figure 6. The processes responsible for these two decay rates are not yet clear. The $Py^+$ decay may be governed by recombination with trapped electrons. In considering these results, it is important to keep in mind that the ice processes described here are recorded for one temperature (10 K) and will most likely depend on temperature.

## 5. ASTROPHYSICAL IMPLICATIONS

Water is by far the dominant component of interstellar ices. Since PAHs are considered to be widespread throughout the ISM, they are likely to be frozen out wherever $H_2O$-rich ices are present. The photochemical dynamics observed here and the new spectroscopic information make two astrophysical points.

Astrochemically, this work shows that the effective photolytic production of PAH ions in PAH containing ice upon VUV irradiation should not be neglected a priori when modeling interstellar ice chemistry. The behavior of the various species that is shown in Figure 4 suggests that a new set of solid-state reactions appears when irradiating PAH containing water ice. The present study is on a rather isolated ice system—typical for this type of laboratory study—comprising Py and $H_2O$. In a more realistic interstellar sample, containing other constituents, such as CO, $CO_2$ or $NH_3$, and other PAHs, chemical pathways will become more complicated, but since water is the most

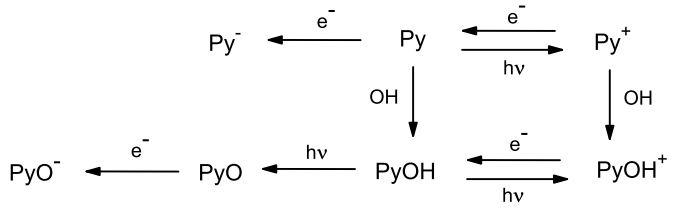


**Figure 5.** Possible reactions upon photolysis of Py:$H_2O$ ice as derived from Figure 3.

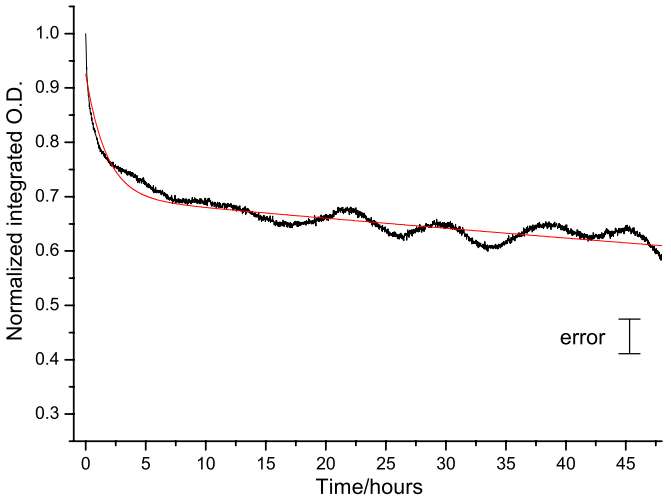


**Figure 6.** Normalized pyrene cation integrated OD as a function of time plotted together with a double exponential fit using Equation (3) (red curve). The wiggles superposed on the signal are caused by baseline effects and fall within the error of 5% as indicated by the error bar.

(A color version of this figure is available in the online journal.)

dominant component in these extraterrestrial ices, we expect that the trends observed here will generally apply. Another important point to note is that reactions involving ions are not included in any of the current astrochemical grain chemistry networks. The present study shows that positive ions can reside in the ice mantle for a substantial time. This is particularly interesting since an astronomical dust grain is a truly isolated system, whereas the laboratory analogue is grown on the tip of a cold finger.

Observationally, the spectroscopic results provide an alternative route to search for PAH features in space. Astrophysical searches to identify PAHs and PAH cations in the ISM/CSM have focused on vibrational and electronic transitions in the gas phase as well as solid-state PAH features in the infrared. As stated previously, these searches have been largely unsuccessful. The infrared work suffers from spectral congestion and spectral overlap of vibrational modes. This prohibits an unambiguous identification of an emission feature to a specific carrier. In the UV/VIS this is partly overcome as electronic excitations are unique for different PAHs. However, electronic spectra of gas phase PAHs showed no overlap with absorption features recorded through diffuse interstellar clouds, presumably of too low column densities (Romanini et al. 1999; Bréchignac & Pino 1999). A different situation applies in the solid state; PAHs are refractory material and accumulate in time onto cold grains that offer a reservoir. Therefore, the specific embedding of PAHs in water ice as presented here provides an alternative starting point for an astronomical search. However, one has to realize that this idea has both pros and cons.

Table 1 shows that under the present experimental conditions the bands are rather broad. The FWHM of the $Py^+$ absorption

feature at 445.6 nm is 66 Å. From an observational point of view this has the advantage that profiles can be studied at medium resolution, but also goes with the challenge to correct very accurately for possible background signals and in the end spectral overlaps may still exist, e.g., with silicate or carbonaceous features. Nevertheless, overlapping broad bands can contribute to the very broad structure (VBS) superposed on the interstellar extinction curve (Hayes et al. 1973; van Breda & Whittet 1981; Krelowski et al. 1986) and simply may have been overlooked in the past.

As stated before, the electronic excitation energy is unique. This is good for selectivity, but bad for sensitivity, since spectral features of different PAHs do not add up (as in the infrared) and consequently an individual optical band strength is, in principle, directly determined by the actual abundance of one specific PAH in space. It is difficult, however, to predict the percentage of the total interstellar PAH population that might exist in the form of one specific PAH, e.g., pyrene. Nevertheless, electronic PAH transitions are typically 2–3 orders of magnitude stronger than their IR bands and from this point of view, we expect that PAH bands may be observable in the visible even though IR bands are barely discernible on the strong $H_2O$ bands (Brooke et al. 1999). This is also reflected by the very good S/Ns as visible in Figure 2 for a very diluted mixture. We expect PAHs to be sufficiently abundant in ices in regions of molecular clouds with $A_v \geqslant 8$ to permit detection in the optical. Infrared ice bands have been detected along such lines of sight and the visible extinction is low enough to permit UV from the interstellar radiation field to process these ices.

We have estimated the expected Py and $Py^+$ absorption band strength toward an example source, MWC297. This is an early-type B1.5V star with a well-characterized stellar spectrum, a $B$ magnitude of 14.34 and a 3.0 $\mu$m ice band with $\tau = 0.04$. Using the high sensitivity of an 8 m class telescope (VLT) it is feasible to obtain, within a couple of hours, S/N $\geqslant$ 1000 spectra of such a highly extincted source in the wavelength range under investigation. To estimate the expected OD of a pyrene or pyrene cation ice absorption we use the standard relation:

$$N_{\rm H}/E(B-V) = 5.8 \times 10^{21} \text{ atoms cm}^{-2} \text{ mag}^{-1} \qquad (4)$$

from Bohlin et al. (1978). With $E(B-V) = 2.67$ toward MWC297 (Drew et al. 1997) this results in $N_{\rm H} = 1.6 \times 10^{22}$ cm$^{-2}$. Taking the total PAH abundance in clouds with respect to $n_{\rm H}$ to be $\sim 3 \times 10^{-7}$, this results in a total PAH column density of $9.6 \times 10^{15}$ cm$^{-2}$. Assuming that 1% of the total PAHs in space is in the form of pyrene frozen out on grains and of this fraction up to 10% is in its singly ionized state ($Py^+$), the total column density of $Py^+$ or Py toward MWC297 is estimated to range between $9.6 \times 10^{12}$ and $8.64 \times 10^{13}$ species cm$^{-2}$. The OD is defined as

$$\tau = \frac{NA}{\Delta\nu}, \qquad (5)$$

with $N$ the column density of the absorbers, $A$ the integrated band strength, and $\Delta\nu$ the FWHM. For a typical strong allowed vibronic transition, such as the $^1B_{2u} \leftarrow {}^1A_g$ Py and $^2A_u \leftarrow {}^2B_{3g}$ $Py^+$ transitions, we take $A_{\rm Py} = 2.9 \times 10^{-13}$ cm molecule$^{-1}$ and $A_{\rm Py^+} = 2.9 \times 10^{-13}$ cm radical$^{-1}$ in ice with a FWHM = 400 cm$^{-1}$ and 300 cm$^{-1}$, respectively. This yields ODs of $0.01 \leqslant \tau \leqslant 0.06$ for Py and $Py^+$, respectively, a range similar to that observed for ice bands.

## 6. CONCLUSION

This work presents the first results of a spectroscopic and photochemical study of pyrene in water ice upon VUV irradiation under astronomical conditions. Since the spectra are recorded in real time, it is possible to derive photochemical characteristics and to monitor a rich ion-mediated chemistry in the solid state. Such processes are yet to be considered in astrochemical models. Additionally, it is shown that the pyrene cations formed within the $H_2O$ ice by VUV irradiation remain trapped in the ice for an extended period. Successive heating of the ice makes these ions available to diffusing species and hence should be considered in the solid-state astrochemical processes.

The new laboratory approach presented here offers a general way to provide astronomically relevant PAH solid-state spectra. Specifically, the spectra discussed here provide an alternative way to search for pyrene features in the ISM/CSM. The derived numbers show the potential of this method, but one has to realize, as pointed out before, that these numbers incorporate our limited knowledge on the actual PAH quantities in space. For different PAHs, with different abundances and different absorption strengths other numbers, both less and more favorable, may be expected. Furthermore, it is possible—in view of the rather effective way in which charged species form and stay in the ice—that the actual abundance of ions may be higher. The results presented here are new and aim at a further characterization of the chemical role of PAHs and PAH derivatives in space.

This work is financially supported by "Stichting voor Fundamenteel Onderzoek der Materie" (FOM), "the Netherlands Research School for Astronomy" (NOVA), and NASA's Astrobiology Program. L. J. Allamandola thanks the "Nederlandse Organisatie voor Wetenschappelijk Onderzoek" (NWO) for a visitors grant and NASA's Laboratory Astrophysics and Astrobiology Programs for support.

## REFERENCES

Agúndez, M., et al. 2008, A&A, 478, L19
Allamandola, L. J., Tielens, A. G. G. M., & Barker, J. R. 1989, ApJS, 71, 733
Bernstein, M. P., et al. 1999, Science, 283, 1135
Bisschop, S. E., Fuchs, G. W., van Dishoeck, E. F., & Linnartz, H. 2007, A&A, 474, 1061
Bito, Y., Shida, N., & Toru, T. 2000, Chem. Phys. Lett., 328, 310
Bohlin, R. C., Savage, B. D., & Drake, J. F. 1978, ApJ, 224, 132
Boogert, A. C. A., et al. 2008, ApJ, 678, 985
Bréchignac, P., & Pino, T. 1999, A&A, 343, L49
Brooke, T. Y., Sellgren, K., & Geballe, T. R. 1999, ApJ, 517, 883
Cernicharo, J., et al. 2001, ApJ, 546, L123
Draine, B. T., et al. 2007, ApJ, 663, 866
Drew, J. E., et al. 1997, MNRAS, 286, 538
Elsila, J. E., Hammond, M. R., Bernstein, M. P., Sandford, S. A., & Zare, R. N. 2006, Meteorit. Planet. Sci., 41, 785
Fuchs, G. W., et al. 2009, A&A, submitted
Gillett, F. C., Forrest, W. J., & Merrill, K. M. 1973, ApJ, 183, 87
Gudipati, M. 2004, J. Phys. Chem. A, 108, 4412
Gudipati, M. S., & Allamandola, L. J. 2003, ApJ, 596, L195
Gudipati, M. S., & Allamandola, L. J. 2004, ApJ, 615, L177
Gudipati, M. S., & Allamandola, L. J. 2006, ApJ, 638, 286
Halasinski, T. M., Salama, F., & Allamandola, L. J. 2005, ApJ, 628, 555
Hayes, D. S., Mavko, G. E., Radick, R. R., Rex, K. H., & Greenberg, J. M. 1973, in IAU Symp. 52, Interstellar Dust and Related Topics, ed. J. M. Greenberg & H. C. van de Hulst (Dordrecht: Kluwer), 83
Hirata, S., Lee, T., & Head-Gordon, M. 1999, J. Chem. Phys., 111, 8904
Hudgins, D. M., Sandford, S. A., Allamandola, L. J., & Tielens, A. G. G. M. 1993, ApJS, 86, 713
Ioppolo, S., Cuppen, H. M., Romanzin, C., van Dishoeck, E. F., & Linnartz, H. 2008, ApJ, 686, 1474

Kim, H.-S., Wagner, D. R., & Saykally, R. J. 2001, Phys. Rev. Lett., 86, 5691
Kjaergaard, H. G., Robinson, T. W., & Brooking, K. A. 2000, J. Phys. Chem. A, 104, 11297
Krelowski, J., Maszkowski, R., & Strobel, A. 1986, A&A, 166, 271
Linnartz, H. 2009, in Cavity Ring-Down Spectroscopy; Techniques and Applications, ed. G. Berden & R. Engeln (New York: Wiley), 145
McCarroll, B. 1970, Rev. Sci. Instrum., 41, 279
Mendoza-Gomez, C. X., de Groot, M. S., & Greenberg, J. M. 1995, A&A, 295, 479
Milosavljevic, B., & Thomas, J. 2002, Photochem. Photobiol. Sci., 1, 100
Miyauchi, N., et al. 2008, Chem. Phys. Lett., 456, 27
Motylewski, T., et al. 2000, ApJ, 531, 312
Muñoz Caro, G. M., et al. 2002, Nature, 416, 403
Öberg, K. I., Linnartz, H., Visser, R., & van Dishoeck, E. F. 2009, ApJ, 693, 1209
Öberg, K. I., et al. 2008, ApJ, 678, 1032
Peeters, Z., et al. 2005, A&A, 433, 583
Puget, J. L., & Leger, A. 1989, ARA&A, 27, 161
Romanini, D., et al. 1999, Chem. Phys. Lett., 303, 165
Ruiterkamp, R., Peeters, Z., Moore, M. H., Hudson, R. L., & Ehrenfreund, P. 2005, A&A, 440, 391
Salama, F., & Allamandola, L. J. 1991, J. Chem. Phys., 94, 6964
Sceats, M. G., & Rice, S. A. 1982, Water: A Comprehensive Treatise, Vol. 7 (New York: Plenum), 83
Smith, J. D. T., et al. 2007, ApJ, 656, 770
Vala, M., et al. 1994, J. Phys. Chem., 98, 9187
van Breda, I. G., & Whittet, D. C. B. 1981, MNRAS, 195, 79
van Broekhuizen, F. A., Pontoppidan, K. M., Fraser, H. J., & van Dishoeck, E. F. 2005, A&A, 441, 249
van Dishoeck, E. F. 2004, ARA&A, 42, 119
Wang, B. C., Chang, J. C., Tso, H. C., Hsu, H. F., & Cheng, C. Y. 2003, J. Mol. Struct. (Theochem.), 629, 11
Watanabe, N., & Kouchi, A. 2002, ApJ, 571, L173